Frequency Analysis of the Combustion Instabilities Induced by a Backward-Facing Step

Stéphane Boulal, Jean-Michel Klein, Yves Fabignon, Axel Vincent-Randonnier, Vladimir Sabelnikov

Frequency Analysis of the Combustion Instabilities induced by a Backward-Facing Step

By Stéphane BOULAL,[1)] Aurélien GENOT,[1)] Jean-Michel KLEIN,[1)]Yves FABIGNON,[1)] Axel VINCENT-RANDONNIER,[2)] and Vladimir SABEL'NIKOV,[1)]

[1)]*DMPE, ONERA, Université Paris Saclay, F-91123, Palaiseau, France*
[2)]*ONERA / DMPE, Université de Toulouse, F-31055, Toulouse, France*

Combustion instabilities are serious issues encountered in several propulsive applications such as rocket engines or aero gas turbines. In the years 2004-2006, ONERA conducted a series of experiments in the LAERTE facility, which aimed at improving the level of understanding of the mechanisms of flame stabilization behind a backward-facing step (BFS), a situation having direct applications to ramjets or afterburners. In this work, we re-analyze the imaging results (visible luminosity and OH* chemiluminescence) obtained at that time with a lean-premixed CH_4/air flame. Three canonical cases are described: *(i)* a Stable Case whereby the flame behaves steadily, *(ii)* a Metastable Case for which the flame manifests moderate excursions upstream of the step, and *(iii)* an Unstable Case by which the flame manifests a periodic flashback. The recording sequences are analyzed by means of the Spectral Proper Orthogonal Decomposition (SPOD) technique in order to extract the space and time coherent motions contained within the dynamics. It is revealed that two main mechanisms are coexistent. The first one, characterized by a frequency f_a, is associated with a longitudinal acoustic resonance of the experimental apparatus. The second one, characterized by a frequency f_h, corresponds to the hydrodynamic instability developing downstream of the step, i.e., that of the flow roll-up induced by the recirculation bubble. When the two frequencies are quite different from one another, the flame is relatively steady and does only flap with soft amplitude. As the difference between the two frequencies narrows down, a hydro-acoustic coupling emerges. This manifests with higher peak amplitudes in the frequency domain and higher motion amplitudes in the space/time domain. When the two frequencies coincide, the situation is favorable for the flashback emergence in that the coupling induces large fluctuations of the flow velocity to the point that it drops below the flame speed.

Key Words: Combustion Instability, Flashback, Backward-Facing Step, Modal Analysis, Hydro-acoustic

Nomenclature

f	:	frequency, Hz
h	:	inlet duct height, m
h_s	:	step height, m
L_c	:	chamber section length, m
L_{in}	:	inlet section length, m
$\dot{m}_{air}$	:	air mass flow-rate, kg/s
$\dot{m}_{CH4}$	:	methane mass flow-rate, kg/s
M_0	:	inlet Mach number
P	:	combustor pressure, bar
St	:	Strouhal number
s_f	:	flame speed, m/s
t	:	time, s
T_0	:	inlet air temperature, K
u	:	axial flow velocity, m/s
u_0	:	inlet flow velocity, m/s
Δ	:	pitch size of the honeycomb grid, m
Δf	:	Hydro-acoustic frequency proximity , Hz
δf	:	SPOD spectrum frequency resolution , Hz
ϕ	:	methane/air mixture equivalence ratio
Subscripts		
1L	:	longitudinal fundamental eigenmode
1Ty, 1Tz	:	transverse fundamental eigenmodes
a	:	acoustic mode
h	:	hydrodynamic mode
KH	:	Kelvin-Helmholtz or step mode

1. Introduction

Flame flashback still constitutes a significant issue in combustion applications[1,2)] where the structural integrity of the combustors may be impacted by the massive motion of the flame towards the injection, in potentially uncooled locations. Furthermore, pressure oscillations resulting from thermo-acoustic feedback can exacerbate this issue. In practical combustion devices, flashback may occur when attempting to stabilize a flame in flows where the bulk velocity is greater than the flame velocity.[3)] In most practical applications, flame anchoring is not feasible without the use of special geometries such as swirlers, bluff-bodies, or backward-facing steps (BFS).[4,5)] These approaches result in flow recirculation, which is intended to produce local stagnation spots, *i.e.*, regions of the flow where the flow velocity u is of the order of the flame speed s_f, thereby encouraging the stabilization of the flame. However, these methods have inherent drawbacks, such as an increased risk of flashback due to vortex breakdown,[6)] core flow flashback,[1)] or boundary layer flashback.[7,8)] Flashback is more likely to occur in the presence of combustion instabilities, where the flame anchoring spot may follow velocity oscillations and propagate towards boundary layers.[9–12)] In the worst case scenario where premixing of the reactants is required and no flame arrestors are implemented usptream of the combustor, the flashback can transit into a detonation, which has even more devastating outcomes. Besides, considering the current trend towards the use of hydrogen (H_2) or hydrogen-enriched fuel in gas-turbine com-

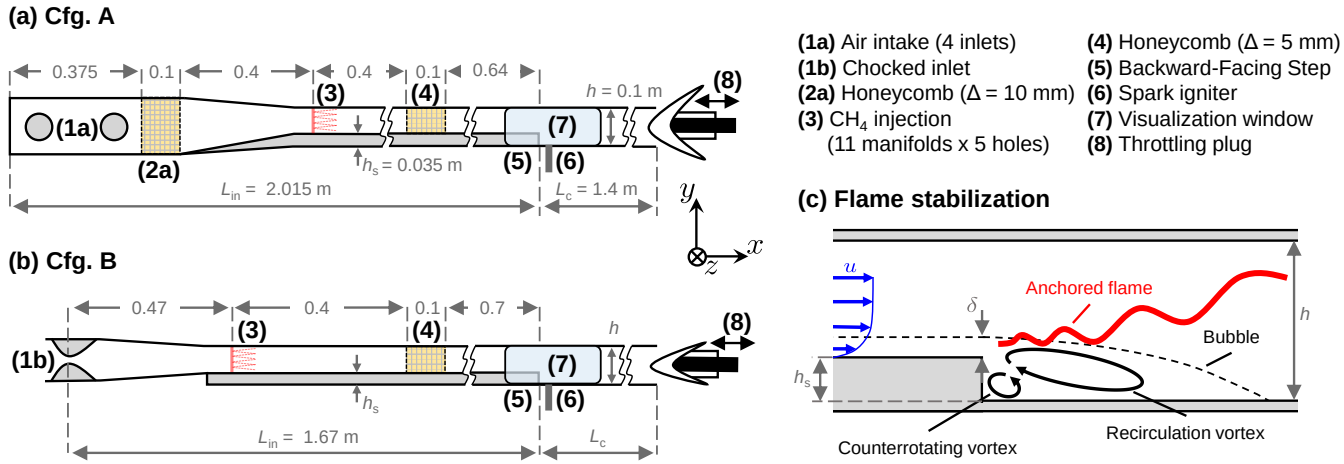

Fig. 1. Schematic views of the Backward-Facing Step ducted-combustor in the Cfg. A **(a)** and Cfg. B **(b)**. The horizontal lengths are not to scale and specified in meter. **(c)** Process of flame stabilization behind the Backward-Facing Step.

bustors, the risk of flame flashback could increase because the speed of hydrogen-fueled flames is typically one order of magnitude greater than that of flames fueled by kerosene[13] or natural gas.[14]

This study re-examines the experimental results gathered at the LAERTE facility of ONERA between 2004 and 2006,[15–18] focusing on a spectral analysis of the recordings of visible luminosity and OH* chemiluminescence of a methane/air premixed flame stabilized in a ducted combustion chamber by means of a BFS. The experimental setup and operating conditions of the cases reported in this study are reviewed in Sect. **2.**. Sect. **3.** describes each case dynamics. A Spectral Proper Orthogonal Decomposition (SPOD) analysis is caried out in Sect. **4.**, wherein the hydro-acoustic coupling specifically responsible for the flashback is discussed.

2. Experimental setup

2.1. Backward-Facing Step ducted-combustor

Two versions of a ducted combustion chamber, labeled as Cfg. A and Cfg. B, were employed in the experiments. Both configurations consist of a tunneled combustion chamber with a Backward-Facing Step located approximately halfway through. This simple design was intended as a tool for the investigation of the mechanisms of flame stabilization behind obstacles, with applications ranging from ramjets to afterburners. Figure 1 schematizes the two configurations as well as the process according to which the flame stabilizes at about the step location. The cross-section of the combustion chamber is 100×100-mm^2. The step height is h_s = 35 mm. Preheated air with a mass flow rate of $\dot{m}_{air}$ is delivered to the combustion chamber via a choked throat located at the front end. The main differences between the two configurations are their acoustic characteristics **(1a or 1b)** and inlet geometry, as well as slight variations in the shape of the throttling plug **(8)**.

In Cfg. A, there is a throat situated upstream of the combustor (which is not shown in Fig. 1). The choked air moves through an intake manifold (a plenum) downstream of the throat before being dispersed to four inlets attached to the ducted combustion chamber **(1a)**. The air then travels through a honeycomb grid with a length of 100 mm and a Δ = 10-mm-pitch length. The primary purposes of the grid are to reduce the level of turbulence generated by the impingement of the four intakes and to straighten the turning flow created by the 90° injection.

Cfg. B was introduced after Cfg. A and features a more streamlined flow pattern upstream of the step, achieved by placing the inlet throat **(1b)** closer to the combustion chamber. The development of a shock train is imposed by the inlet sonic throat as the flow transits from supersonic to subsonic conditions. The acoustic implications of this phenomenon are not well understood, but Culick and Rogers[19,20] suggest modeling it as a normal shock. This shock can be considered a closed acoustic boundary condition, at least to a first-order approximation.

Methane (CH_4) is injected into the inlet duct through 55 regularly spaced holes drilled in five vertical manifolds **(3)**, at the ambient temperature with a mass flow rate of $\dot{m}_{CH4}$. In order to homogenize the flow velocity profile and composition of the resulting methane/air mixture, a 100-mm-long honeycomb grid is employed, with a pitch size of Δ = 5-mm. After the flow passes by the honeycomb grid, its composition can reasonably be considered as uniform with an equivalence ratio $\phi = (\dot{m}_{air}/\dot{m}_{CH4})_{st.}/(\dot{m}_{air}/\dot{m}_{CH4})$, where $(\dot{m}_{air}/\dot{m}_{CH4})_{st.}$ = 17.3 is the stoichiometric air-to-fuel ratio. A spark-igniter **(6)** is flush-mounted to the bottom wall downstream of the BFS **(5)**. In stable operation, the recirculation zone formed downstream of the step and the associated low-velocity zones enable the flame front to stabilize at the tip of the step. The inlet temperature T_0 of the airflow can be adjusted up to 650 K, which is much lower than the auto-ignition temperature of methane/air mixtures, typically in the range of ∼ 800 – 900K.[21] The system is completed with a convergent nozzle **(8)** at the back-end of the combustor. A horizontally traveling throttling plug is employed to vary the throat's surface area, allowing adjustment of the back-end acoustic impedance and chamber pressure P. Two dynamic pressure transducers installed on the top wall measure the pressure oscillations. Their recordings and analyses are provided in Refs.[15–18]

At the location of the step, two quartz windows measuring 260 mm in length and 100 mm in height are installed to allow for lateral visualization. Except for the regions surrounding the visualization windows, the combustion chamber walls are water-cooled. Several optical diagnoses were used in the experimental campaigns, including Particle Image Velocimetry (PIV),[16–18] Planar Laser Induced Fluorescence of the OH Rad-

icals (PLIF-OH) imaging,[15–18] visible luminosity imaging,[15] CH* chemiluminescence imaging[15] and OH* chemiluminescence imaging.[15–18] For the purpose of producing laser sheets for the PIV and PLIF-OH measuring techniques, a third optical access is placed on the top wall. In the following, we revisit the high-speed flame recordings obtained from visible luminosity imaging of Ref.[15] acquired at a 1-kHz-rate and the OH* chemiluminescence imaging of Refs.[15–18] acquired at a 4-kHz-rate. For more information about the visualization methods and equipment used at the time, we refer the readers to the references mentioned above.

2.2. Operating conditions

We investigate three cases where the flame exhibited three distinct behaviors: a stable behavior (Stable Case), a near-stable behavior (Metastable Case), and an unstable behavior, specifically that of periodic flame flashback (Unstable Case). The Unstable Case has already been discussed in Refs.[15–18] and was obtained in Cfg. B, while the Stable and Metastable cases were obtained in Cfg. A. Table 1 lists the operating conditions for each case in terms of the chamber pressure P, inlet air temperature T_0, air mass flow rate $\dot{m}_{\text{air}}$, and the equivalence ratio ϕ of the ideal methane/air mixture. The cross-sectional average inlet velocity u_0, *i.e.*, that prior to the step, is also provided in Table 1. The fundamental eigenfrequencies obtained for the

Table 1. Experimental conditions (averaged values) of the cases reported, $\boldsymbol{P}$: combustor time-averaged pressure, $\boldsymbol{T_0}$: inlet air temperature, $\boldsymbol{\dot{m}_{\text{air}}}$: air mass flow-rate, $\boldsymbol{\phi}$: methane/air mixture equivalence ratio, $\boldsymbol{u_0}$: inlet velocity, $\boldsymbol{M_0}$: inlet Mach number.

Case	Stable	Metastable	Unstable
Cfg.	A	A	B
$\boldsymbol{P}$ **(bar)**	1.05	1.44	1.35
$\boldsymbol{T_0}$ **(K)**	460	460	550
$\boldsymbol{\dot{m}_{\text{air}}}$ **(kg/s)**	0.28	0.28	0.27
$\boldsymbol{\phi}$	0.82	0.82	0.82
$\boldsymbol{u_0}$ **(m/s)**	59	44	51
$\boldsymbol{M_0}$	0.14	0.10	0.11

limiting models of a closed/open tube (*i.e.*, a quarter-wave resonance) and a closed/closed tube (*i.e.*, a half-wave resonance) are provided in Table 2 for the three cases considered. The eigenfrequencies were obtained from an acoustic modeling, as described in Ref.[22] As the flow is not choked at the outlet of the combustion chamber, the measured acoustic eigenfrequencies should be closer to the values calculated using the closed/open model. In terms of transverse eigenmodes in the y and z directions, the fundamental mode frequencies can be framed such that $3310 < f_{1\text{T}y} < 3620$ Hz and $2150 < f_{1\text{T}z} < 2350$ Hz upstream of the step, and $4400 < f_{1\text{T}y} = f_{1\text{T}z} < 4445$ Hz downstream of the step.

Table 2. Framing of the fundamental eigenfrequency $f_{1\text{L}}$ for the three cases between the limiting acoustic models of the closed-open tube (quarter-wave resonance) and the closed-closed tube (half-wave resonance).

Case	Stable	Metastable	Unstable
Cfg.	A	A	B
Closed-open tube			
$f_{1\text{L}}$ **(Hz)**	35	36	44
Closed-closed tube			
$f_{1\text{L}}$ **(Hz)**	80	81	99

3. Results

In this section, we provide a qualitative description of the flame dynamics observed in each of the three cases. Snapshots of the recordings for each case are shown in Figure 2.

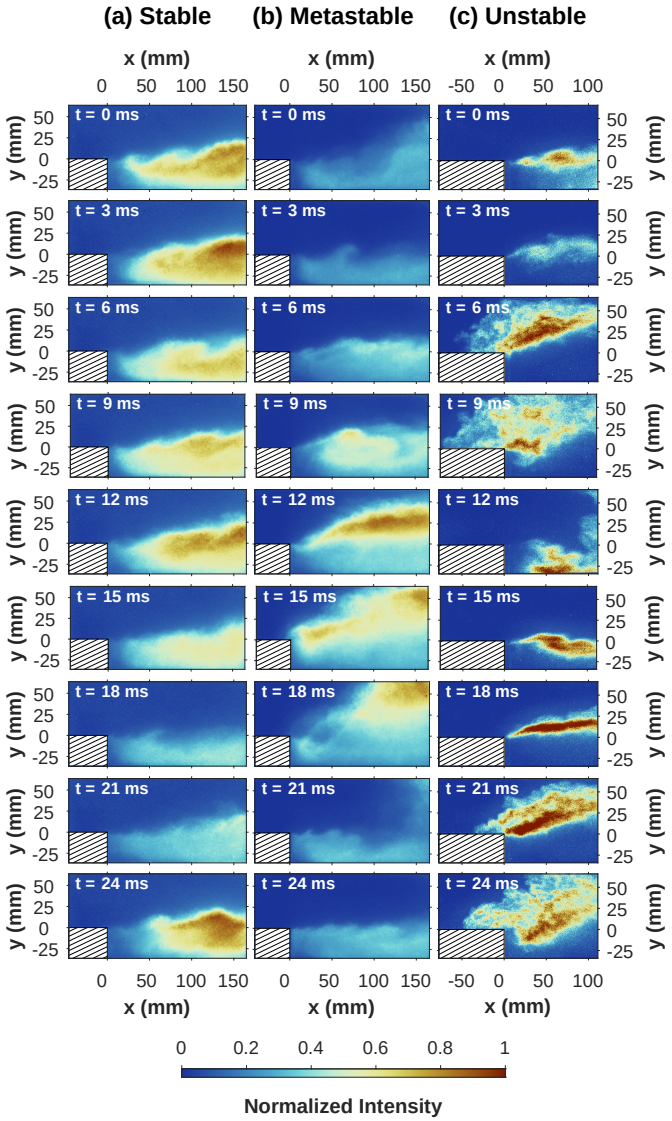

Fig. 2. Fluctuations of the normalized flame intensity captured by means of visible luminosity **(a, b)** or OH* chemiluminescence **(c)** high-speed imagings for the Stable **(a)**, Metastable **(b)** and Unstable **(c)** cases. The time-step between each frame is 3 ms. The dashed box on the bottom left corner represents the Backward-Facing Step.

For the Stable Case (Fig. 2(a)), the flame stabilizes about the shear layer trailing in the wake of the step. The flame front, *i.e.*, the interface separating burnt gases from fresh gases, is wrinkled by shedded vortices as a result of the density and velocity gradients across the shear layer (often referred to as Kelvin-Helmholtz instability[23]). This may be clearly seen on the time frame $t = 0$ ms of Fig. 2(a). The flame motion observed in the Stable Case can be considered as a combination of the *stable* and *buzzing* cases reported by Keller *et al.*[24]

For the Metastable Case (Fig. 2(b)), the flapping motion of the flame is already quite noticeable. We observe that the flame briefly propagates upstream of the step tip between $t = 12$ and

t = 15 ms. One could consider this event to be a mild flashback. In qualitative terms, the flame motion observed in the Metastable Case bears resemblance to the *buzzing* case reported in Ref.[24)]

For the Unstable Case (Fig. 2(c)), the upstream propagation of the flame is now much more significant. Yet, the amplitude of motion fluctuates. In some cycles, it extends far beyond the visualizations window. The flame flashback event appears to result from a threshold-induced disruption of the rather progressive flame oscillation, as observed in the time frames t = 6 and t = 21 ms. This point will be further discussed in §**4.3.**. Qualitatively, the flame motion observed in the Unstable Case is similar to the *chucking* case described by Keller *et al.*[24)]

4. Spectral analysis

In this section, we delve deeper into the processes outlined in the previous section. To do so, we use the Spectral Proper Orthogonal Decomposition (SPOD) method to analyze the flame motion. This technique decomposes the flame motion into coherent orthogonal modes in both space and time, with the aim of extracting the processes responsible for the flame motion. The SPOD technique, in the form derived by Towne *et al.*,[25)] seeks to extract coherent mechanisms from processes that may otherwise appear chaotic. The frequency spectrum returned by the SPOD technique is limited to $f < 0.5$ kHz with a $\delta f \approx 1.5$ Hz-frequency-resolution for the Stable and Metastable cases (visible luminosity imaging imaging composed of 1018 snapshots recorded at a 1 kHz-acquisition rate), and $f < 2$ kHz with $\delta f \approx 0.5$ Hz for the Unstable Case (OH* chemiluminescence imaging composed of 12282 snapshots recorded at a 4 kHz-acquisition rate).

4.1. Stable Case

The spectral density distribution estimated by the SPOD for the Stable Case is shown in Figure 3(a). Two peaks of small amplitudes stand out from the background at frequencies f = 45 Hz and f = 73 Hz. The shapes computed for these two modes are given in Fig. 3(b) and (c), respectively. The shape of the first mode suggests that the flame front is flapping vertically at a frequency f = 45 Hz. This flapping instability is similar to that of a flame anchored at the lip of a coaxial rocket injector, as described in Ref.[26)] The frequency of this mode falls between the two limiting values determined in §**2.2.** (also shown in Table 2): $35 < f < 80$ Hz, more closely to the closed-open model of a quarter-wave resonance. This indicates that the flapping motion is related to an acoustic resonance, and is henceforth referred to as f_a. From a phenomenological standpoint, this mode can be understood as the result of the flame's interaction with a planar vertical wave (i.e., the acoustic wave), which causes the flame to move in the same direction as the wave propagates through it.

The shape of the second mode, occurring at the frequency f = 73 Hz, suggests the flame front wrinkling and roll-up inside the recirculation bubble. This phenomenon is indicative of a hydrodynamic instability, and we refer to this mode frequency as f_h. The instability is characterized by a Strouhal number St_h, which is based on the step height h_s and the bulk flow velocity u_0. We obtain a value of $St_h = f_h h_s / u_0 = 0.0433$.

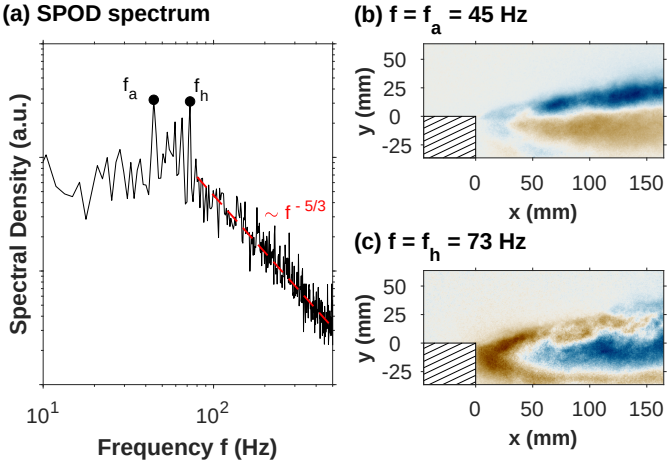

Fig. 3. **(a)** SPOD spectrum of the recordings for the Stable Case. **(b)** SPOD shape of the f = 45-Hz mode. **(c)** SPOD shape of the f = 73-Hz mode.

4.2. Metastable Case

The spectral density distribution estimated by the SPOD for the Metastable Case is shown in Figure 4(a). Here, four peaks with greater amplitudes standing out from the background are observed: the first one at f = 46 Hz, the second one at f = 52 Hz, the third one at f = 94 Hz and the last one at f = 148 Hz. The shapes obtained for each of these four modes are shown in Figure 4(b), (c), (d) and (e), respectively. At higher frequencies, the spectrum follows a power law with an exponent −3. It would seem plausible to relate this to the inertial range observed in two-dimensional turbulence,[27)] for which the vorticity flow occurs at small scales. For the Stable Case (see Fig. 3), the turbulence is three-dimensional (including in the shear layer). As such, the spectrum follows the classical −5/3 power law proposed by Kolmogorov for the turbulent energy spectra.[28)]

The mode shape at the frequency f = 46 Hz exhibits qualitative similarity to the mode associated with the acoustic resonance observed for the Stable Case. Once more, the frequency of this mode falls between the two limiting values determined in §**2.2.** (also refer to Table 2): $36 < f < 81$ Hz. Hence, it is reasonable to assume that this mode corresponds to the longitudinal acoustic resonance. As the sound speed does not differ much between the Stable and Metastable cases, there is no specific reason for the natural frequencies of the combustor to change from one case to another.

On the other hand, the velocity u_0 significantly differs between the two cases (see also Table 1). As such, the mode at the frequency f = 52 Hz (Fig. 4(c)) corresponds to a Strouhal number St_h = 0.0414, which is within 5% of the value determined for the Stable Case, demonstrating that the identified hydrodynamic instability is self-similar. The flame flapping is amplified by the emergence of a coupling between two distinct mechanisms both inducing an up-and-down motion of the flame. The first one relates to the acoustic resonance evoked above. The second relates to the flame roll-up induced by the recirculation bubble (the hydrodynamic instability). This mechanism, described in the works of Keller *et al.*,[24)] Altay *et. al.*[29,30)] or Hong *et. al*[31)] is sketched in Figure 5. The flame roll-up results in fresh gases trapped between the combustor wall and the re-

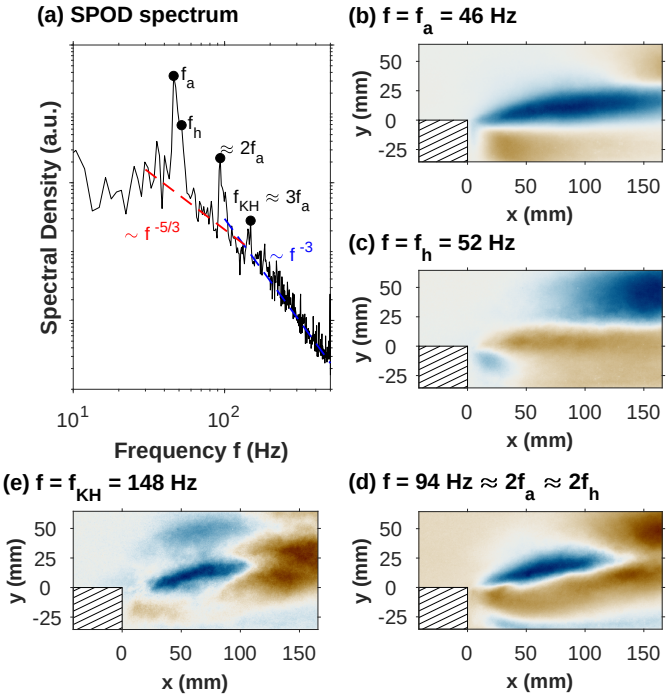

Fig. 4. **(a)** SPOD spectrum of the recordings for the Metastable Case. **(b)** SPOD shape of the $f = 46$-Hz mode. **(c)** SPOD shape of the $f = 52$-Hz mode. **(d)** SPOD shape of the $f = 94$-Hz mode. **(e)** SPOD shape of the $f = 148$-Hz mode.

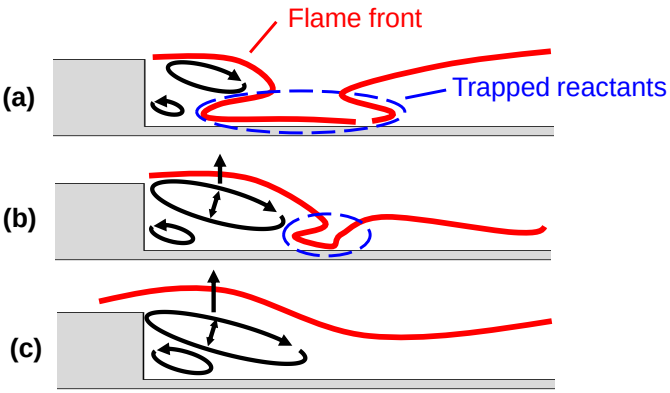

Fig. 5. Schematic view of the flame roll-up and bubble dilatation mechanisms favoring the onset of a flashback. **(a)** trapped reactants, **(b)** burning of the fresh gas pocket leading to dilatation, **(c)** upward motion of the flame and tendency for it to flashback in the boundary layer.

circulation bubble (a). These fresh gases then react leading to the overall dilation of the bubble (b). In response, this entails the vortices and the flame front to ascent above the step (c) and the latter is enticed to flashback in the boundary layer. This complex flow pattern is well captured by the shape of the mode at the $f = 52$ Hz-frequency. The intensity of the hydro-acoustic coupling is governed by the proximity between the two frequencies associated to each mechanism: $\Delta f = |f_a - f_h| = 6$ Hz. The coupling explains the widening of the spectum on the right side of the peak at $f = f_a$. It is also responsible for the overall higher amplitude computed on the frequency domain as well as the larger motion amplitude observed in the time-domain.

The mode at the frequency $f = 94$ Hz (Fig. 4(d)) lies between $2f_a = 92$ Hz and $2f_h = 104$ Hz. Clearly, the associated shape is a manifestation of the hydro-acoustic coupling. The shape of this mode suggests a combination of the acoustic and hydrodynamic motions. It is worth noting that the peak at $2f_a$ is unexpected in a combustor modeled as a closed-open tube, where only odd multiples of the fundamental frequency should be excited. It follows that the first harmonic should be located at $f_{2L} = 3f_{1L}$. For instance, such a quarter-wave resonance was observed in the oxygen feed line of a rocket-type combustion chamber in Ref.[26] The excitation of both even and odd harmonics is indicative of a non-linear behavior.

Finally, the mode at $f = 148$ Hz (Fig. 4(d)), which appears to contain the majority of the flame wrinkling, is definitely that of a Kelvin-Helmholtz type instability. The SPOD shape reveals a wave-packet structure similar to that observed in other works, such as those of Refs.[25,26] The Strouhal number corresponding to the frequency $f = f_{KH} = 148$ Hz is $St_{KH} = 0.118$, which is consistent with literature values for this well-known "step mode".[23,32–34] This mode stands out from the background since its frequency falls between $3f_a$ and $3f_h$. This Kelvin-Helmholtz instability produces quasi-2D vertical structure followed by stochasticization and vorticity cascade to smaller scales (larger frequencies). This explains *a posteriori* the -3 power law trend obtained for $f \gtrsim f_{KH}$.

4.3. Unstable Case

Figure 6(a) shows the spectral density distribution computed by the SPOD for the Unstable Case, which reveals up to six frequency peaks located at multiples of the fundamental frequency, $f = 67$ Hz. The peaks are even more pronounced than in the previous cases. Qualitatively, this corresponds to the larger flame motion amplitudes observed for this case. The shapes computed for the two first modes are shown in Fig. 4(b) and (c). The fundamental mode is still falling within the range determined in §**2.2.** (see also Table 2): $44 < f_a < 99$ Hz. The hydrodynamic and acoustic modes now seem to be fully coupled, as evidenced by a single peak at $f_a \approx f_h$ resulting from the shift of both frequencies to a common value. Considering that this severe coupling occurs because $f_a \approx f_h$, then we may estimate the Strouhal number of the instability as $St_h = 0.0460$, which is within 6 and 10% of what was obtained for the Stable and Metastable cases, respectively. At higher frequencies, the spectrum is here closer to the $-5/3$ power law, because the heat release zone,*i.e.*, the flame front, moves as a whole with the 3D turbulence contained within it.

To summarize, the flame flashback is caused by the amplification of the flapping motion of the flame, which is induced by both the longitudinal acoustic resonance at the frequency f_a, and the hydrodynamic instability associated to the flame roll-up at the frequency f_h. The occurrence of the flashback results from the coincidence of the step position with a velocity anti-node imposed by the hydro-acoustic coupling, *i.e.*, a position where the velocity is subjected to the highest amplitude of fluctuations. This then cause the flow velocity to fall below the flame speed, thereby triggering the flashback event. This argument is quantitatively addressed in Ref.[22] Still, we provide its main outcomes in the following.

Figure 7 shows a selection of snapshots chosen at a regular intervals over one oscillation period. The flashback motion starts at $t \approx 3.5$ ms, which is when u (modeled based on the PIV measurements reported in Refs.[16–18]) drops below $s_f \approx 16$ m/s, as evaluated in Ref.[22] The flashback motion ends at $t \approx 8.25$ ms

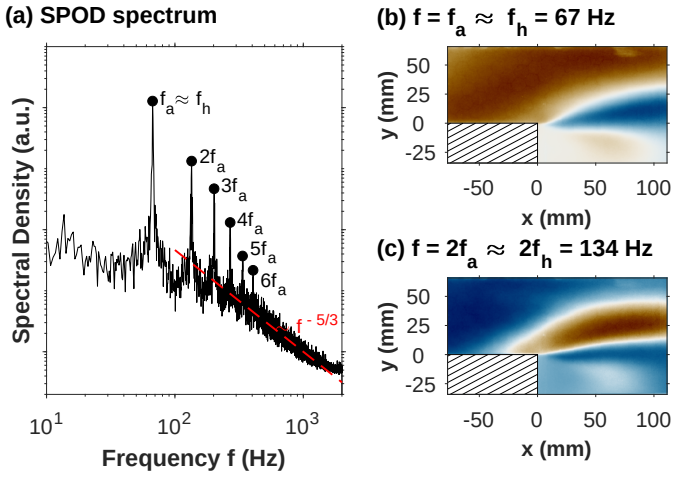

Fig. 6. **(a)** SPOD spectrum of the recordings for the Unstable Case. **(b)** SPOD shape of the f = 67-Hz mode. **(c)** SPOD shape of the f = 134-Hz mode.

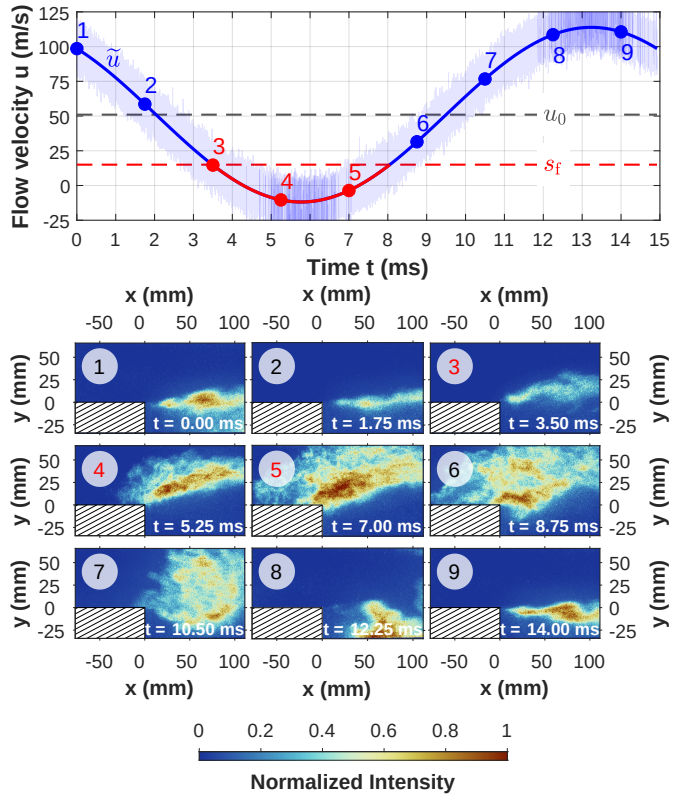

Fig. 7. Illustration of the flashback cycle within one oscillation period. The top graph allows for comparison between the velocity u of the flow and the assumed value for the flame speed s_f = 15 m/s. The solid line represents the turbulence-filtered evolution.

when the bulk of the OH* intensity stops flowing in the negative x direction, which is consistent with the moment when $u > s_f$. The flame is driven downstream as the flow velocity increases, stabilizing away from the step for a moment. The time when the velocity reaches its maximum, which is $t \approx 13$ ms, also coincides with the most downstream position of the flame in Figure 7.

It is important to note that these observations complete the interpretations put forward in Refs.[16–18] At the time, the flashback motion was thought to be caused by a flow reversal. However, based on the current study, it has been determined that the flashback is a result of the flow velocity dropping below the flame speed, and it could still occur even if the flow velocity remained positive.

During some flashback cycles, such as the one shown in Figure 8, we notice the spontaneous creation of an auto-ignition front on the top wall, which is believed to result from the temporal low-velocity found in this location, particularly in the boundary layer, and the presence of a local hot spot on the top wall surface. The hot spot at this position can be attributed to two reasons. On the one hand, it may be due to the rise in wall temperature caused by earlier flashback cycles. Secondly, it may be due to localized hot spots that are impeded by uneven cooling of the combustor walls, particularly at the junction where the top uncooled quartz window (used for the PLIF and PIV laser sheets, not presented in this article) meets the water-cooled wall onto which the window is mounted. The auto-ignition event occurs with a probability of approximately 3%, as it has only been observed six times out of the 205 flashback cycles recorded. A similar phenomenon is reported in Refs.,[35,36] where the authors studied the re-initiation of a tube-confined detonation from a decoupled shock-flame complex. Such a process appeared to be stochastic in that the re-initiation could occur either at corners or walls of the tube due to Mach reflections of transverse shock waves, or within the cross-section upon the collision of two transverse waves.

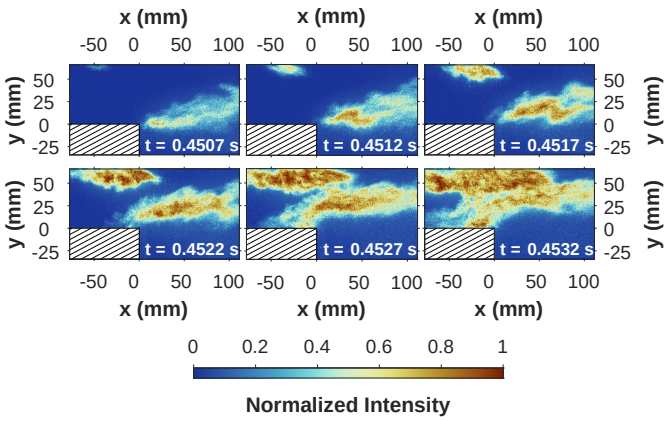

Fig. 8. Auto-ignition front spontaneous generation during a flashback cycle.

5. Conclusions

In this sudy, we aimed to gain a comprehensive understanding of the flashback mechanism of a premixed flame in a duct equipped with a Backward-Facing Step. Our approach is based on the spectral analysis of the high-speed recordings of an experimental database that was collected at ONERA some years ago. The SPOD technique was used so as to decompose the flame motion into its main components. We found that the flame dynamics could reduce to two main mechanisms: an acoustic resonance and a hydrodynamic instability. We observed that the flame is stable when the characteristic frequencies associated with each component are far apart, but becomes unstable as the frequencies approach each other, resulting in a moderate upstream excursion of the flame front upstream of the step. The hydro-acoustic coupling is complete when the two

frequencies coincide. Consequently, the flow velocity fluctuations imposed by the hydro-acoustic coupling become so much amplified that the flame speed can supersede it, prompting the flashback. The hydrodynamic instability related to the flame roll-up motion is identified with a Strouhal Number based on the step height h_s and the bulk flow velocity u_0 to a value $\mathrm{St_h} = f_h h_s / u_0 = 0.044 \pm 5\%$.

The presence or absence of a thermo-acoustic feedback could not be determined. Further research is needed to understand the cycle-to-cycle change observed in the motion amplitude and the underlying governing equation describing the flashback limit-cycle. One potential expansion of this work involves studying the system's bifurcation dynamics by ramping up or down the Equivalence Ratio ϕ, the inlet temperature T_0, or the combustor pressure P to characterize the transient evolutions from the Stable Case dynamics to the Unstable Case dynamics.

Acknowledgments

This work was funded by ONERA, the French Aerospace Lab. We gratefully acknowledge Ajmal K. Mohamed, Joel Dupays, Laurent Jacquin, Philippe Villedieu, Jérôme Anthoine and Olivier Dessornes for their continuous support in the research of combustion dynamics.

References

1) T. Lieuwen, V. McDonell, D. Santavicca, T. Sattelmayer, Burner development and operability issues associated with steady flowing syngas fired combustors, Combustion Science and Technology 180 (6) (2008) 1169–1192.
2) T. Lieuwen, V. McDonell, E. Petersen, D. Santavicca, Fuel flexibility influences on premixed combustor blowout, flashback, autoignition, and stability, J. Eng. Gas Turbines Power 130 (1) (2008).
3) R. J. Kee, M. E. Coltrin, P. Glarborg, H. Zhu, Chemically reacting flow: theory, modeling, and simulation, John Wiley & Sons, 2017.
4) P.-H. Renard, D. Thevenin, J.-C. Rolon, S. Candel, Dynamics of flame/vortex interactions, Progress in energy and combustion science 26 (3) (2000) 225–282.
5) K. S. Kedia, A. F. Ghoniem, The anchoring mechanism of a bluff-body stabilized laminar premixed flame, Combustion and flame 161 (9) (2014) 2327–2339.
6) M. Konle, F. Kiesewetter, T. Sattelmayer, Simultaneous high repetition rate piv–lif-measurements of civb driven flashback, Experiments in Fluids 44 (2008) 529–538.
7) V. Kurdyumov, E. Fernandez, A. Linan, Flame flashback and propagation of premixed flames near a wall, Proceedings of the Combustion Institute 28 (2) (2000) 1883–1889.
8) V. Hoferichter, C. Hirsch, T. Sattelmayer, Prediction of confined flame flashback limits using boundary layer separation theory, Journal of Engineering for Gas Turbines and Power 139 (2) (2017).
9) Y. Sommerer, D. Galley, T. Poinsot, S. Ducruix, F. Lacas, D. Veynante, Large eddy simulation and experimental study of flashback and blow-off in a lean partially premixed swirled burner, Journal of Turbulence 5 (1) (2004) 037.
10) D. Ebi, N. T. Clemens, Experimental investigation of upstream flame propagation during boundary layer flashback of swirl flames, Combustion and Flame 168 (2016) 39–52.
11) D. Thibaut, S. Candel, Numerical study of unsteady turbulent premixed combustion: Application to flashback simulation, Combustion and Flame 113 (1-2) (1998) 53–65.
12) J.-M. Klein, A. Genot, A. Vincent-Randonnier, A. Mura, Combustion thermoacoustics: on the relevance of some stability criteria, in: 9th European Conference For Aeronautics And Space Sciences EUCASS-3AF, 2022.
13) Y. Wu, V. Modica, X. Yu, F. Grisch, Experimental Investigation of Laminar Flame Speed Measurement for Kerosene Fuels: Jet A-1, Surrogate Fuel, and Its Pure Components, Energy & Fuels 32 (2) (2018) 2332–2343.
14) N. Donohoe, A. Heufer, W. K. Metcalfe, H. J. Curran, M. L. Davis, O. Mathieu, D. Plichta, A. Morones, E. L. Petersen, F. Güthe, Ignition delay times, laminar flame speeds, and mechanism validation for natural gas/hydrogen blends at elevated pressures, Combustion and Flame 161 (6) (2014) 1432–1443.
15) V. Sabel'nikov, F. Grisch, M. Orain, Instabilities and structure of turbulent premixed flame in a lean stepped combustor, in: 17th International Society for Air Breathing Engines (ISABE) Conference, Munich, Germany, 2005.
16) V. Sabel'nikov, C. Brossard, M. Orain, F. Grisch, M. Barat, A. Ristori, P. Gicquel, Thermo-acoustic instabilities in a backward-facing step stabilized lean-premixed flame in high turbulence flow, in: 14th International Symposium on Applications of Laser Techniques to Fluid Mechanics, 2008.
17) C. Brossard, V. Sabel'nikov, M. Orain, F. Grisch, M. Barat, A. Ristori, P. Gicquel, Etude expérimentale des instabilités thermo-acoustiques d'une flamme turbulente prémélangée, in: Congrès Francophone de Techniques Laser, 2008.
18) V. Sabel'nikov, C. Brossard, M. Orain, F. Grisch, M. Barat, A. Ristori, P. Gicquel, Visualization study of thermo-acoustic instabilities in a backward-facing step stabilized lean-premixed flame in high turbulence flow, in: 10th Conference (International) on Fluid Control, Measurements, and Visualization (FLUCOME)), 2009.
19) F. Culick, T. Rogers, The response of normal shocks in diffusers, AIAA journal 21 (10) (1983) 1382–1390.
20) E. Bekaert, A. Genot, T. Le Pichon, T. Schuller, Low-order models for acoustic modes in a ramjet combustor with inlet shock train, in: 9th European Conference For Aeronautics And Space Sciences EUCASS-3AF, 2022.
21) R. Bounaceur, P.-A. Glaude, B. Sirjean, R. Fournet, P. Montagne, M. Vierling, M. Molière, Prediction of Auto-Ignition Temperatures and Delays for Gas Turbine Applications, Journal of Engineering for Gas Turbines and Power 138 (2) (2016) 021505.
22) S. Boulal, A. Genot, J.-M. Klein, Y. Fabignon, A. Vincent-Randonnier, V. Sabel'nikov, On the hydro-acoustic coupling responsible for the flashback limit-cycle of a premixed flame at a backward-facing step, under review (2023).
23) D. Wee, S. Park, T. Yi, A. Annaswamy, A. Ghoniem, Reduced order modeling of reacting shear flow, in: 40th AIAA Aerospace Sciences Meeting & Exhibit, 2002, p. 478.
24) J. O. Keller, L. Vaneveld, D. Korschelt, G. L. Hubbard, A. F. Ghoniem, J. W. Daily, A. K. Oppenheim, Mechanism of instabilities in turbulent combustion leading to flashback, AIAA Journal 20 (2) (1982) 254–262.
25) A. Towne, O. T. Schmidt, T. Colonius, Spectral proper orthogonal decomposition and its relationship to dynamic mode decomposition and resolvent analysis, J. Fluid Mech. 847 (2018) 821–867.
26) S. Boulal, N. Fdida, L. Matuszewski, L. Vingert, M. Martin-Benito, Flame dynamics of a subscale rocket combustor operating with gaseous methane and gaseous, subcritical or transcritical oxygen, Combust. Flame 242 (2022) 112179.
27) R. H. Kraichnan, Inertial Ranges in Two-Dimensional Turbulence, The Physics of Fluids 10 (7) (1967) 1417–1423.
28) A. N. Kolmogorov, The local structure of turbulence in incompressible viscous fluid for very large reynolds number 30 (1941) 301–303.
29) H. M. Altay, R. L. Speth, D. E. Hudgins, A. F. Ghoniem, Flame–vortex interaction driven combustion dynamics in a backward-facing step combustor, Combust. Flame 156 (5) (2009) 1111–1125.
30) H. M. Altay, R. L. Speth, D. E. Hudgins, A. F. Ghoniem, The impact of equivalence ratio oscillations on combustion dynamics in a backward-facing step combustor, Combust. Flame 156 (11) (2009) 2106–2116.
31) S. Hong, S. J. Shanbhogue, R. L. Speth, A. F. Ghoniem, On the phase between pressure and heat release fluctuations for propane/hydrogen flames and its role in mode transitions, Combustion and Flame 160 (12) (2013) 2827–2842.
32) K.-B. Chun, H. J. Sung, Control of turbulent separated flow over

a backward-facing step by local forcing, Experiments in fluids 21 (1996) 417–426.
33) H. N. Najm, A. F. Ghoniem, Coupling between vorticity and pressure oscillations in combustion instability, Journal of Propulsion and Power 10 (6) (1994) 769–776.
34) D. M. Driver, H. L. Seegmiller, J. G. Marvin, Time-dependent behavior of a reattaching shear layer, AIAA journal 25 (7) (1987) 914–919.
35) S. Boulal, Comportements dynamiques de la détonation dans des compositions gazeuses non-uniformes, Ph.D. thesis, École Nationale Supérieure de Mécanique et d'Aérotechnique (ENSMA) (2017).
36) S. Boulal, P. Vidal, R. Zitoun, T. Matsumoto, A. Matsuo, Experimental investigation on detonation dynamics through a reactivity sink, Combustion and Flame 196 (2018).